Invited Paper

The Hand-Held Directional Reflectometer: An angular imaging device to measure BRDF and HDR in real-time

Phillip Mattison, Mark Dombrowski, Jim Lorenz

Surface Optics Corporation
11555 Rancho Bernardo Road, San Diego, CA 92127-1441

Keith Davis, Ph. D., Harley Mann, Philip Johnson

Boeing Defense and Space Group
P.O. Box 3707, Seattle, WA 98124

Bryan Foos

Air Force Research Laboratory
Wright Patterson AFB, OH 45433

ABSTRACT

Many applications require quantitative measurements of surface light scattering, including quality control on production lines, inspection of painted surfaces, inspection of field repairs, etc. Instruments for measuring surface scattering typically fall into two main categories, namely bi-directional reflectometers, which measure the angular distribution of scattering, and hemispherical directional reflectometers, which measure the total scattering into the hemisphere above the surface. Measurement of the bi-directional reflectance distribution function (BRDF) gives the greatest insight into how light is scattered from a surface. Measurements of BRDF, however, are typically very lengthy measurements taken by moving a source and detector to map the scattering. Since BRDF has four angular degrees of freedom, such measurements can require hours to days to complete. Instruments for measuring BRDF are also typically laboratory devices, although a field-portable bi-directional reflectometer does exist. Hemispherical directional reflectance (HDR) is a much easier measurement to make, although care must be taken to use the proper methodology when measuring at wavelengths beyond 10 μm, since integrating spheres (typically used to make such measurements) are very energy inefficient and lose their integrating properties at very long wavelengths. A few field-portable hemispherical directional reflectometers do exist, but typically measure HDR only at near-normal angles.

Boeing Defense and Space Group and Surface Optics Corporation, under a contract from the Air Force Research Laboratory, have developed a new hand-held instrument capable of measuring both BRDF and HDR using a unique, patented angular imaging technique. A combination of an hemi-ellipsoidal mirror and an additional lens translate the angular scatter from a surface into a two-dimensional spatial distribution, which is recorded by an imaging array. This configuration fully maps the scattering from a half-hemisphere above the surface with more than 30,000 angularly-resolved points and update rates to 60 measurements per second. The instrument then computes HDR from the measured BDR. For ease of use, the instrument can also compare both the BRDF and HDR to preset limits, generating a Pass/Fail indicator for HDR and a high-acceptable-low image display of BRDF. Beam incidence elevation is variable from normal incidence ($\theta = 0°$) to 5° off grazing ($\theta = 85°$), while scattering is measured to nearly 90° off normal. Such capability is extremely important for any application requiring knowledge of surface appearance at oblique viewing angles. The current instrument operates over the range of 3 μm to 12 μm, with extension into the visible band possible.

Part of the SPIE Conference on Scattering and Surface Roughness II
San Diego, California • July 1998

SPIE Vol. 3426 • 0277-786X/98/$10.00

1.0 DESCRIPTION OF THE HHDR

The Hand-Held Directional Reflectometer (HHDR) was designed to make *in situ* measurements of the infrared (IR) reflection properties of materials in field environments. The instrument consists of a 7.75 lb. hand-held measurement head, which is connected by a 25-foot cable to a rugged portable computer as shown in Figure 1-1. The instrument is self-contained, with power provided by batteries located in the computer and no need for cryogenic materials such as liquid nitrogen. Calibration can be verified in the field, by measuring a reference standard provided with the instrument. The HHDR can be used by a single operator, but in some situations, it may be more convenient to have two operators; one for the measurement head and one for the computer.

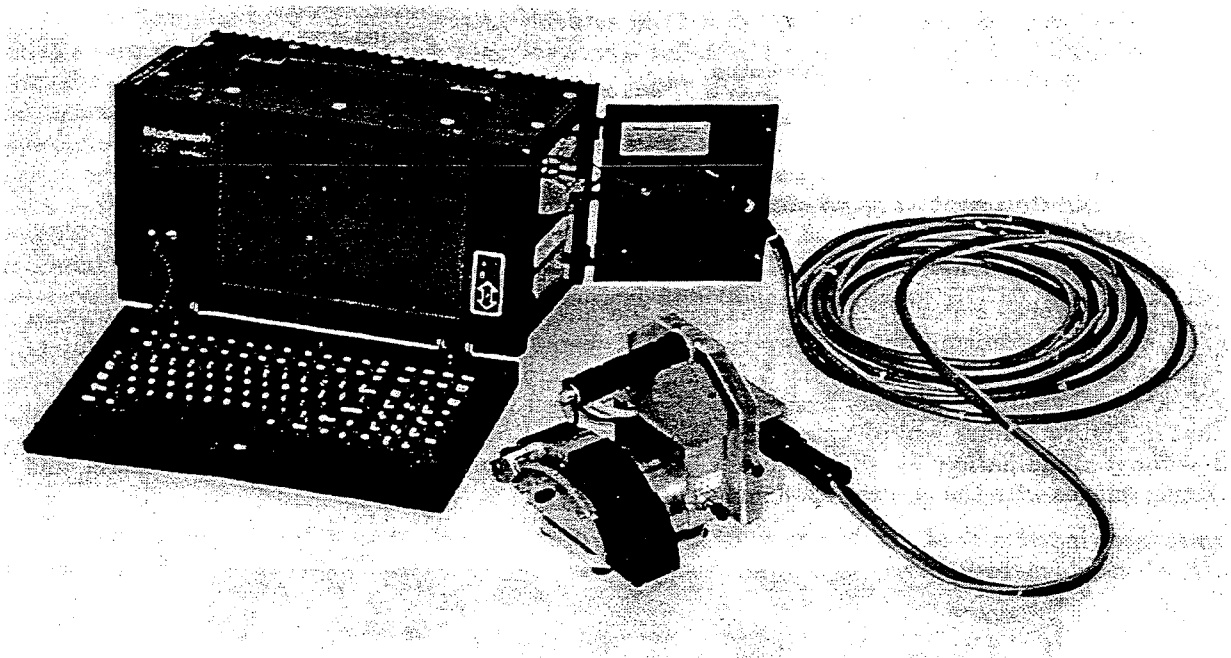

Figure 1-1 - The HHDR consists of a measurement head and portable computer, which are connected by a 25-foot cable.

When the HHDR head is placed in contact with a material to be measured, a small region of the surface, about 4 sq. mm, is illuminated by a broad-band, infrared beam at a user-established angle of incidence. IR light, which is scattered from the surface, is directed, by an ellipsoidal mirror and lens combination, onto an IR imaging focal plane array (FPA) as illustrated in Figure 1-2.

Each pixel in the "angular image" formed on the array corresponds to a small range of scattering angles relative to the illuminated spot on the measured surface. See Figure 1-3. If the detector response is known for each pixel, the images may be interpreted as a quantitative measurement of the angular distribution of the reflected light. Alternatively, if we divide by the incident intensity of the illuminating beam, we may think of the images as revealing the angular distribution of reflectance from the sample. By summing over the image, we may determine the total reflectance, though this is complicated by the fact that not all scattered rays are captured in the image.

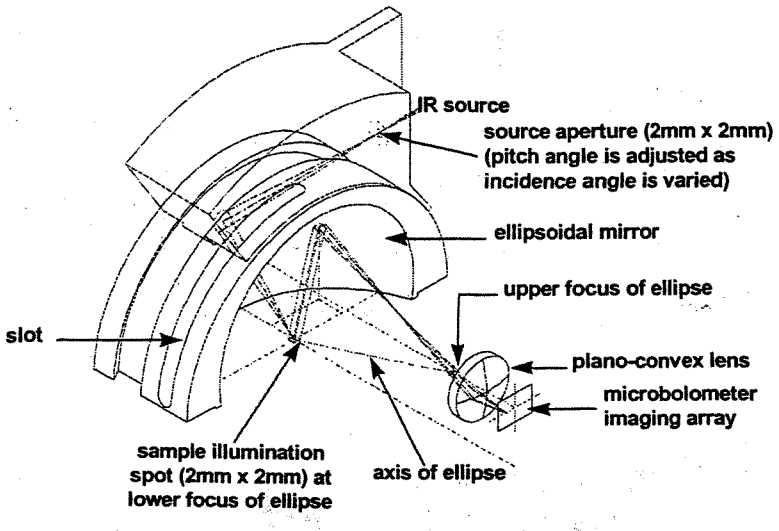

Figure 1.2 – Patented Optics of the HHDR. Parallel rays leaving the illuminated spot at an arbitrary angle are brought to a point at the focal plane array.

The microbolometer FPA that measures the angular image has been fitted with a custom window with good transmission for wavelengths between 3 and 12 microns. The HHDR uses filters to restrict measurements to either the 3 - 5 or 8 - 12 micron bands. In these wave bands there are significant background emissions from the instrument and the sample. Consequently, images such as that in Figure 1-3 are actually produced by taking the difference between images produced with and without illumination by the IR beam. This is accomplished by shuttering the beam and collecting images with the shutter open and closed.

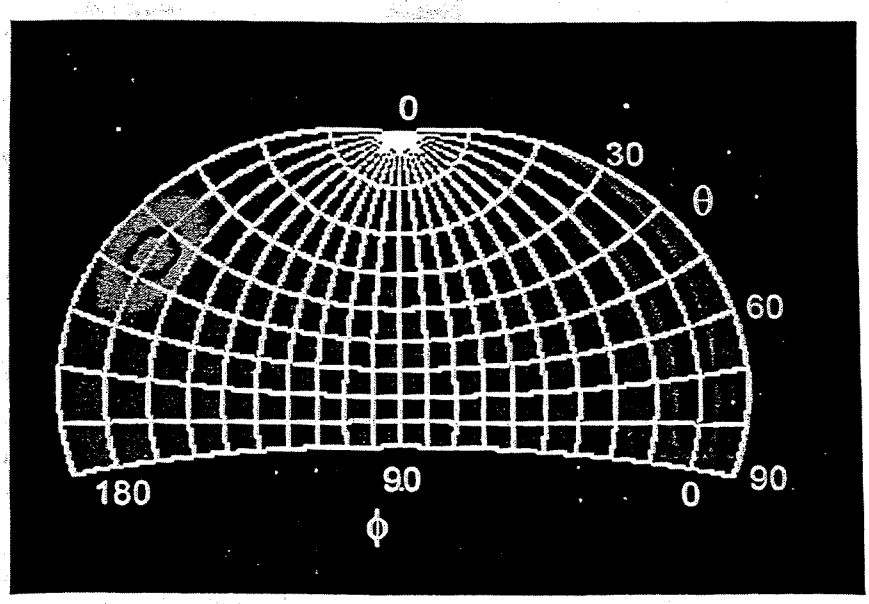

Figure 1-3 - Angle image formed by the HHDR showing 3-5 μm reflected light distribution for an incidence angle of 45°.

Readout and control of the array, offset correction and analog-to-digital conversion are accomplished by four electronics cards located in the measurement head. Digital image data is delivered via the cable to a processor expansion card in the computer, which performs pixel-by-pixel calibration corrections, image subtraction, frame averaging, image re-mapping, and DR computation. The computer also houses expansion cards used for control of the IR source and the shutter. Since most of the processing is done on the various electronics cards, the computer (PC-clone with Windows 95) mainly serves as a human-machine interface, allowing for control of system settings and data collection, and display and storage of data.

2.0 THEORY OF MEASUREMENT

Reflections from smooth metallic surfaces are familiar to most people and are described by Snell's Law of Reflection. This law specifies that a reflected ray lies in the plane of incidence[1] and that the incident and reflected angles[2] are equal. When this law is satisfied, the reflection is said to be "specular." In general, the power in the reflected beam will vary with the incidence angle. This is quantified in terms of the reflection coefficient, the ratio of reflected to incident power.

Other materials, especially rough surfaces, can produce diffuse reflections, which are more complex. In general, reflected rays may be at any angle in the 2π steradian solid angle above the material surface and are properly described by an angular distribution. For these materials, the total reflectance is described by the hemispherical directional reflectance (HDR), at a particular incidence angle. The HDR is the reflected power integrated over all outgoing angles divided by the incident power. Many materials exhibit reflectivity, which is part specular and part diffuse. Much of the reflected power resides in a specular lobe, centered on a specularly reflected ray, with the remaining diffuse component broadly distributed in angle space. Typically for these materials, the specular lobe width narrows and the reflection becomes less diffuse as the incidence angle is increased.

The most general way to describe reflectivity is in terms of the bi-directional reflectance distribution function (BRDF), which is given for specific incident and reflected angles by the following equation:

$$BRDF(\theta_i,\phi_i,\theta_r,\phi_r) = \frac{L(\theta_r,\phi_r)}{\Phi(\theta_i,\phi_i)} \tag{2.1}$$

L is the reflected radiance, measured in watts/(steradian-cm^2), and Φ is the incident flux, measured in watts/cm^2. In this expression, θ is the polar angle and ϕ is the azimuth angle and the subscripts i and r refer to incident and reflected. An equivalent and more intuitive expression for the BRDF, is given by

$$BRDF(\theta_i,\phi_i,\theta_r,\phi_r) = \frac{dP_r / \; d\Omega_r(\theta_r,\phi_r)}{P_i(\theta_i,\phi_i)\cdot\cos(\theta_r)} \tag{2.2}$$

In this expression, P_i is the total incident power and dP_r is the power reflected into the differential solid angle, $d\Omega_r$, at θ_r and ϕ_r. This can be thought of as the reflectance per unit projected[3] solid angle or, in other words, as the distribution of reflectance (multiplied by $1/\cos\theta r$) over the angle space

[1] The plane of incidence contains the incident ray and the surface normal.
[2] The incident and reflected angles are measured from the surface normal.
[3] Projected solid angle refers to $\Omega_r \cdot \cos(\theta_r)$.

above the surface. Insight into this choice of definitions can be obtained by considering the case of idealized Lambertian reflectors for which the brightness of the material in reflection is independent of view angle. For these cases, the power per unit solid angle falls off as $\cos(\theta_r)$, but this is compensated by the reduction in the projected area of the illuminated spot. Consequently, for Lambertian materials, the BRDF is given by a single constant, independent of angle. For the other extreme of a specular reflector, the BRDF is given simply by a delta function times a coefficient, which can depend on incident angle.

In spite of the mathematical simplification, which arises from the inclusion of the $(1/\cos(\theta_r))$ factor in the BRDF definition, we find that it confuses the interpretation of visually displayed BRDF data. Consequently, we actually plot $BRDF \cdot \cos(\theta_r)$, which effectively removes this factor.

The hemispherical directional reflectance (HDR) can be computed from the BRDF by the following integral:

$$HDR(\theta_i,\phi_i) = \int_{\substack{Upper \\ Hemisphere}} BRDF(\theta_i,\phi_i,\theta_r,\phi_r)\cdot\cos(\theta_r)\cdot d\Omega_r(\theta_r,\phi_r). \tag{2.3}$$

The HDR is related to another material property, the directional emissivity, $\varepsilon(\theta,\phi)$, which is the ratio of the actual power radiated by a material in the direction (θ,ϕ) to that of an ideal blackbody. For opaque materials, the directional emissivity and HDR are related by Eq. 2.4.

$$\varepsilon(\theta,\phi) = 1 - HDR(\theta,\phi) \tag{2.4}$$

Thus a measurement of the BRDF over all incident and outgoing angles is equivalent to a full measurement of the directional emissivity of the material.

Most materials are "isotropic", which means that their reflection properties are the same for all azimuthal orientations or, equivalently, for all θ_is. Even for these materials, full characterization of the BRDF, by traditional means, with a movable detector can be very time consuming. Consequently, a more limited set of BRDF measurements, referred to as "ring" and "slice" scans, is usually made for a series of fixed incident angles. A ring scan refers to measured BRDF values corresponding to fixed θ_r, for example, at the same angle as the specular ray, and a series of ϕ_r values on either side of the specular ray. A slice scan is similar except that ϕ_r is fixed and θ_r is varied. Since the HHDR produces an image in the reflected angle space, it already contains substantially more data than ring and slice scans. However, equivalent scan data can be extracted from the HHDR images.

We have not explicitly referred to wavelength (λ) in any of the above definitions and equations. In all cases, they should be interpreted as correct for each individual wavelength. However, they are also correct for waveband averaged quantities and it is these cases that we must consider. In particular, the HHDR measures band averaged quantities in the midwave band, from 3-5 microns, and the longwave band, from 8-12 microns. Other bands could be chosen by an appropriate choice of filters. In practice, the spectral weighting functions, $G(\lambda)$, used in the band averaging is the product of the source spectral power distribution $W(\lambda)$, filter transmission $T(\lambda)$ and detector (microbolometer) response $R(\lambda)$, where $W(\lambda)$ also includes the source window transmission and $R(\lambda)$ incorporates the vacuum dewar window transmission. As an example, the 8 – 12 micron band-averaged value for the BRDF is as follows:

$$BRDF_{(8-12)} = \frac{\int_8^{12} BRDF(\lambda) \cdot G(\lambda) \cdot d\lambda}{\int_8^{12} G(\lambda) \cdot d\lambda} \text{ where } G(\lambda) = W(\lambda) \cdot T(\lambda) \cdot R(\lambda) \qquad (2.5)$$

In order to obtain calibrated BRDF data from angular images, such as that shown in Figure 1-3, we need to determine the reflection angles and solid angle associated with each pixel. This is done by overlaying an angle grid onto the array image. The grid was made by computing trajectories for rays launched from the lower focus and propagated through the optical system comprised of the ellipsoidal mirror, lens, filter and array. The grid is formed by connecting the points, where the rays strike the array, for rings and slices at 10 degree intervals. Therefore, the grid shows how the reflected angle space is mapped onto the array.

Care must be taken to correctly overlay this grid on the FPA image. Slight discrepancies between the ideal and actual optical geometry are dealt with by allowing the grid to be translated and scaled both horizontally and vertically. To facilitate this process, crosshairs corresponding to the ellipsoidal mirror fiducial marks are added to the grid. Translation and scaling factors are then adjusted to obtain a good overlap of the fiducial marks in the FPA image and crosshairs. Generally, scaling factors are within a few percent of 1.00 and the translations of a few pixels are sufficient to provide a good matchup.

Upon studying the grid, it becomes evident that the polar angle becomes compressed for larger θ values. Similarly, the azimuthal angle is stretched when moving away from the ϕ=90 grid line at the center of the image. This angle space distortion means that the solid angle subtended by each pixel in the FPA varies substantially over the image.

This effect could be corrected by numerically computing each pixel's subtended solid angle and then normalizing. After such a correction, the image would correctly display the $BRDF \cdot \cos(\theta)$ image except for a global scale factor. The scale factor could then be determined by using a diffuse calibration standard, illuminated at θ=0, and integrating over the image to obtain an apparent HDR value. The scale factor is then simply the known calibrated HDR value divided by the apparent HDR value. This approach assumes that a response or gain correction[4] has been applied to each pixel. Any variations in optical transmission would show up as BRDF variation.

In practice, we have used a different approach to correcting for pixel solid angle non-uniformity. We again use a well-characterized isotropic BRDF standard, illuminated at θ_i=0, for which we believe we accurately know the BRDF value as a function of θ_r. For each pixel, we determine an expected BRDF based on a computed θ_r and table look-up and interpolation. We then compute a correction factor required to convert the actual pixel contents to the expected $BRDF \cdot \cos(\theta)$ value. This constitutes the calibration process and the correction factors are stored and applied to all subsequent images. This calibration approach automatically corrects for variations in pixel solid angle, detector element response, and optical transmission. It does, however, ignore any possible graininess to the scattered light distribution from the calibration standard.

Once these calibration factors have been applied, each pixel must be weighted by its subtended solid angle when summing over a region to find an integrated reflectance value.[5] This approach is used, for example, when computing HDR values. For isotropic materials, the HDR

[4] Since the BRDF images are actually obtained as a difference of two images (shutter open and shutter closed), it is not necessary to do apply an offset correction to each pixel.

[5] This is accomplished by computing the Jacobian for the transformation between the polar coordinates at the sample and the x-y coordinates of the focal plane array. See Section 2.1

value is found by performing a weighted sum over the region enclosed by the ϕ=0, ϕ=180, and θ=90 grid lines and multiplying by 2. Actually, in order to avoid errors associated with precisely dividing specular peaks with the ϕ=180 grid line, we sum from ϕ=0 to ϕ=170 and add half of the sum from ϕ=170 to ϕ=190. Similarly, the lost contribution, associated with the mirror slot, is dealt with by adding the contribution from ϕ=0 to ϕ= -10. This latter approximate correction is helpful for improving the calibration, but may be the source of a small uncertainty (< 0.5%) in the HDR value.

Another issue to consider in interpreting the images is the angular resolution. This is a somewhat complicated issue due to the fact that the BRDF is a function of four angles. In the input angle space the angular resolution is fairly straight-forward. A cone-like ray bundle is defined by the source slit and the aperture. For the two apertures supplied with the HHDR, the full cone angles are approximately 5.0 ° and 2.5 °. For measurements of specular materials, we would expect to see a specular peak in the image at least as wide as the input beam. The input angle space resolution could be further improved by reducing the size of the slit and aperture, but this will be at the cost of reduced signal-to-noise ratio. In principle, the angular resolution limit is set by the pixel size and image magnification. As can be estimated from Figure 1-3, on average, each pixel is around 0.5 degrees on a side. However, since there are dead spaces between the pixels (65 % fill factor), it is important that a specular spot be several times as wide as a pixel, so that the fraction of lost energy is more-or-less independent of position on the array.

Optical aberrations also affect the angular resolution. For an infinitesimal, illuminated spot at the lower focus, each exit angle from the target is associated with a single point in the image. However, as the spot size is increased, parallel rays, distributed over the spot, are not all brought to exactly the same point in the image. The resulting angular blurring varies significantly over the image and depends strongly on the positioning of the lens and array. In essence, the angular image can not all be brought into "focus" simultaneously.

2.1 Calculation of HDR from BRDF in the UFPA coordinate system

As discussed above, the Bidirectional Reflectance Distribution Function (BRDF), is a function of four variable, namely θ_i, the incident zenith angle, ϕ_i, the incident azimuth angle, θ_r, the reflected zenith angle, and ϕ_r, the reflected azimuth angle. For simplicity, in the following discussion the dependence of BRDF on the incident direction will be understood, but not shown explicitly, such that BRDF is written as $\rho(\theta,\phi)$. Here, θ and ϕ are understood to represent the reflected angles. With this understanding, hemispherical directional reflectance, HDR, is related to BRDF by

$$HDR = \int_{\phi=0}^{2\pi} \int_{\theta=0}^{\pi} \rho(\theta,\phi) \sin\theta \cos\theta \, d\theta \, d\phi \tag{2.6}$$

The optical system of the HHDR transforms the coordinate system in which the BRDF is measured from the three-dimensional polar coordinates used to define BRDF, (θ, ϕ, $\rho(\theta, \phi)$), to a three dimensional Cartesian coordinate system on the UFPA, (x, y, ρ(x, y)). A new equation is required to compute HDR in the UFPA coordinate system.

Since the optical system of the HHDR simply transforms the polar coordinate system at the sample to a Cartesian coordinate system at the array, generation of the new equation is straight forward. In the coordinate system of the array, θ and ϕ are functions of the (x, y) position of a given pixel, such that

$$\theta = \Theta(x,y)$$
$$\phi = \Phi(x,y) \tag{2.7}$$

where Θ and Φ represent the transformation functions from the array coordinates back to the sample polar coordinates. By now determining the Jacobian determinant, J(x,y) (or $\partial(\Theta,\Phi)/\partial(x,y)$), of the Θ, Φ transformation, HDR can be calculated in the UFPA coordinate system.

The Jacobian determinant of a transformation can be viewed as the function that defines the mapping of a unit differential area in one coordinate system to an area in the second coordinate system, i.e., as the "area magnification" function. In the case of the HHDR, the Jacobian determinant defines how a differential area in the polar domain, $d\theta d\phi$, translates to a differential area in the Cartesian domain. Given the above transformations from one coordinate system to the other, this translation is given by

$$d\theta d\phi = J(x,y)dxdy \tag{2.8}$$

where the Jacobian determinant, J(x,y), is given explicitly by

$$J(x,y) = \left| \frac{\partial\Theta(x,y)}{\partial x}\frac{\partial\Phi(x,y)}{\partial y} - \frac{\partial\Theta(x,y)}{\partial y}\frac{\partial\Phi(x,y)}{\partial x} \right| \tag{2.9}$$

Computation of the HDR in the UFPA's Cartesian coordinate system is now a simple matter of substitution into the original equation for determining HDR:

$$HDR = \int_{\Phi(x,y)=0}^{2\pi}\int_{\Theta(x,y)=0}^{\pi} \rho(\Theta(x,y),\Phi(x,y))\sin\Theta(x,y)\cos\Theta(x,y)J(x,y)dxdy \tag{2.10}$$

or, since Θ and Φ are unnecessary in showing the dependence of BRDF on x and y in the UFPA's coordinate system,

$$HDR = \int_{\Phi(x,y)=0}^{2\pi}\int_{\Theta(x,y)=0}^{\pi} \rho(x,y)\sin\Theta(x,y)\cos\Theta(x,y)J(x,y)dxdy \tag{2.11}$$

Since the coordinate system of the UFPA is sampled discretely by the pixels of the UFPA, the above integral translates to the numerical approximation of

$$HDR = \sum_{(x,y)\in(0\le\Phi\le2\pi,\,0\le\Theta\le\pi)}\sum \rho(x,y)\sin\Theta(x,y)\cos\Theta(x,y)J(x,y) \tag{2.12}$$

where the limits on summation show that all pixels are included for which $0 \le \Phi \le 2\pi$ and $0 \le \Theta \le \pi$. When absolute calibration is performed, calibration factors are generated which convert raw pixel values to $\rho(x,y)\sin\Theta(x,y)\cos\Theta(x,y)J(x,y)$, allowing simple summing of calibrated pixel values to effect integration.

The above equation is correct, but unimplementable, since the optical system collects scattered light over only slightly more than half a hemisphere, or an azimuthal range only slightly greater than $0 \le \Phi \le \pi$ (dependent, of course, on the associated value of Θ). By assuming that the

BRDF is isotropic, i.e., that $\rho(\theta, \phi) = \rho(\theta, 2\pi-\phi)$, the above equation for calculating BRDF in the UFPA's coordinate system can be modified to

$$HDR = 2\sum\sum_{(x,y)\in(0\le\Phi\le\pi,\,0\le\Theta\le\pi)} \rho(x,y)\sin\Theta(x,y)\cos\Theta(x,y)J(x,y) \qquad (2.13)$$

where now x and y are constrained to lie in the set for which $0 \le \Phi \le \pi$ and $0 \le \Theta \le \pi$. This equation is both correct and implementable, but is highly sensitive to alignment errors when viewing samples with a significant specular lobe. The equation assumes that the specular energy is split exactly down the middle, with half in one hemisphere, and half in the other. Any small misalignment in azimuth will cause a significant error in HDR.

To make the computed HDR value tolerant to errors in Φ, the area used in computation of the HDR is extended by 10° beyond the specular direction of $\Phi = 180°$. Extending the area of collection ensures that the vast majority of specular energy is collected for computation of the HDR. But when the numerically evaluated integral for the slightly-greater-than-half hemisphere is computed and multiplied by two, the answer is guaranteed to be wrong, since the specular energy is counted twice. Hence, the computation must be corrected to remove one specular-energy contribution. The final form of the numeric evaluation of the integral translating BRDF to HDR is

$$\begin{aligned} HDR = {} & 2\sum\sum_{(x,y)\in(-10^\circ\le\Phi\le190^\circ,\,0\le\Theta\le90^\circ)} \rho(x,y)\sin\Theta(x,y)\cos\Theta(x,y)J(x,y) \\ & - \sum\sum_{(x,y)\in(170^\circ\le\Phi\le190^\circ,\,0\le\Theta\le90^\circ)} \rho(x,y)\sin\Theta(x,y)\cos\Theta(x,y)J(x,y) \end{aligned} \qquad (2.14)$$

The first summation is computed on the processing expansion board, and includes some 30,000 pixels. Specular correction implemented by the second summation is performed by the software using a much more limited number of pixels. Figure 2-1 shows the product of $\sin(\Theta)\cdot J(x,y)$, and one of the components of the Jacobian.

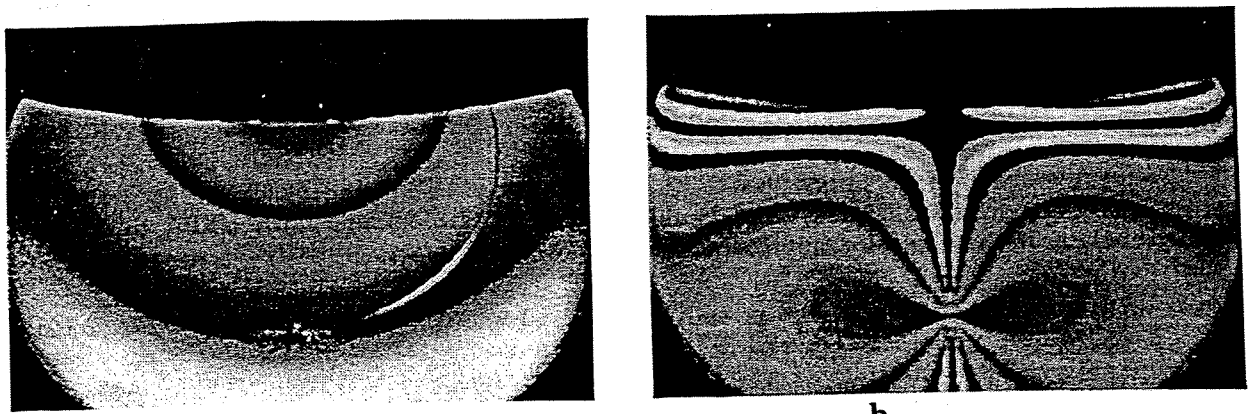

a b

Figure 2-1. a) Map of $\sin\Theta(x,y)\cdot J(x,y)$. b) Map of $\partial\Theta/\partial x$, one of the Jacobian determinant components. (red is the largest value).

3.0 SOFTWARE

A windows-based graphical user interface (GUI) controls operation of the HHDR. All operating parameters and data collection and storage settings are accessible through a series of control buttons and selection boxes on the main interface panel. The main window, displayed when the software is first invoked, contains several controls and displays. Figure 3-1 shows the main window, with each of the following items: Imagery transferred from the DAP to the host computer is displayed in the image display window in the upper left corner of the main window. Immediately below the image display window are two combo boxes, one selecting the image for display, the second selecting the image mapping type. To the right of the image mapping combo box is a third combo box for selecting the display color palette. In the upper right portion of the screen are two status boxes. The first status box displays the computed HDR value, and a PASS/FAIL indicator. To the right of the HDR indicator is a head status box indicating the ambient temperature within the HHDR head, and the temperature of the UFPA. Below these indicators and to the right of the screen are six control buttons for bringing up data entry forms at the bottom of the window for configuring the instrument. Between the control buttons and the image display window are four additional buttons that control display and acquisition of data. Finally, at the bottom right corner of the string is a slider controlling display gain – the factor that imagery from the DAP is scaled by before display.

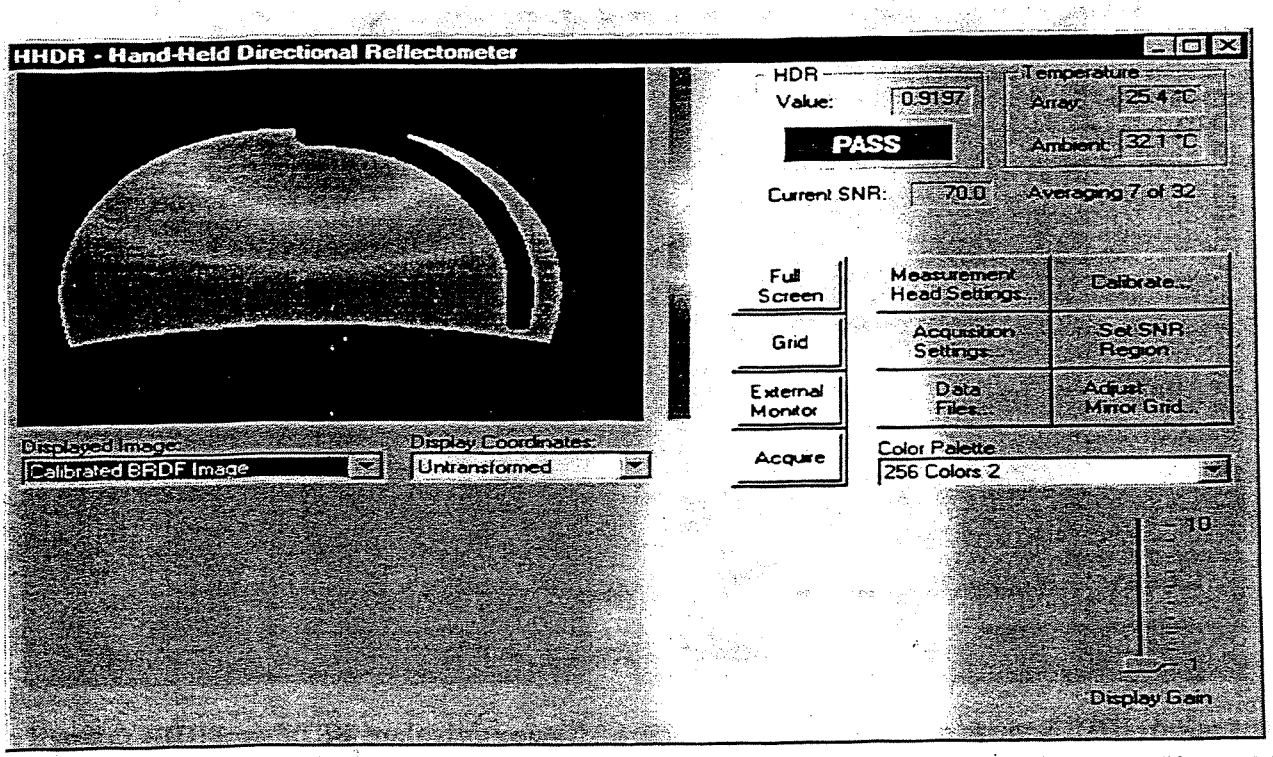

Figure 3.1. HHDR main interface window.

4.0 PERFORMANCE AND MEASUREMENT RESULTS

The array read-out board exhibits an amplifier-noise limit of 0.8 counts, or about 26 μV of UFPA-output referred noise. If the array were used in an F/1.0 imaging system, this equates to amplifier noise equivalent temperature difference (NETD) of 5 mK. In the HHDR, this corresponds

to a noise-equivalent BRDF of about 0.01 sr^{-1} (a 100% Lambertian reflector exhibits a BRDF of $1/\pi$ sr^{-1}, or 0.3 sr^{-1}). Note that this noise is the noise from the amplifier chain alone, excluding the noise contribution of the UFPA itself. The UFPA noise is by far the dominant noise source. Array noise levels measured by BNA are typically about 350 μV. Using the HHDR head electronics module, noise performance improves by about 30%, bringing typical noise levels down to about 250 μV. This noise level corresponds to a noise-equivalent BRDF of about 0.1 sr^{-1}.

Because of the energy-starved nature of the BRDF measurement, frame averaging is a necessity. The processing expansion board allows on-card averaging of up to 256 frames. The HHDR software allows averaging of an unlimited number of output frames from the processing board. At a total averaging of 65,536 frames, noise-equivalent BRDF drops to 0.0004 sr^{-1}. Noise of the HDR computation is significantly less than the BRDF measurement, since upwards of 30,000 pixels are summed in computation of the HDR. HDR noise level, however, does not drop from the BRDF noise level by the square-root of the number of pixels, since some pixel-to-pixel noise correlation exists within a single frame (from, for example, minor temporal variations in array temperature). Averaging 128 frames yields a noise-equivalent HDR value of about 1%. Figure 4-1 shows the interplay between number of averages, noise-equivalent BRDF, noise-equivalent HDR, and measurement time.

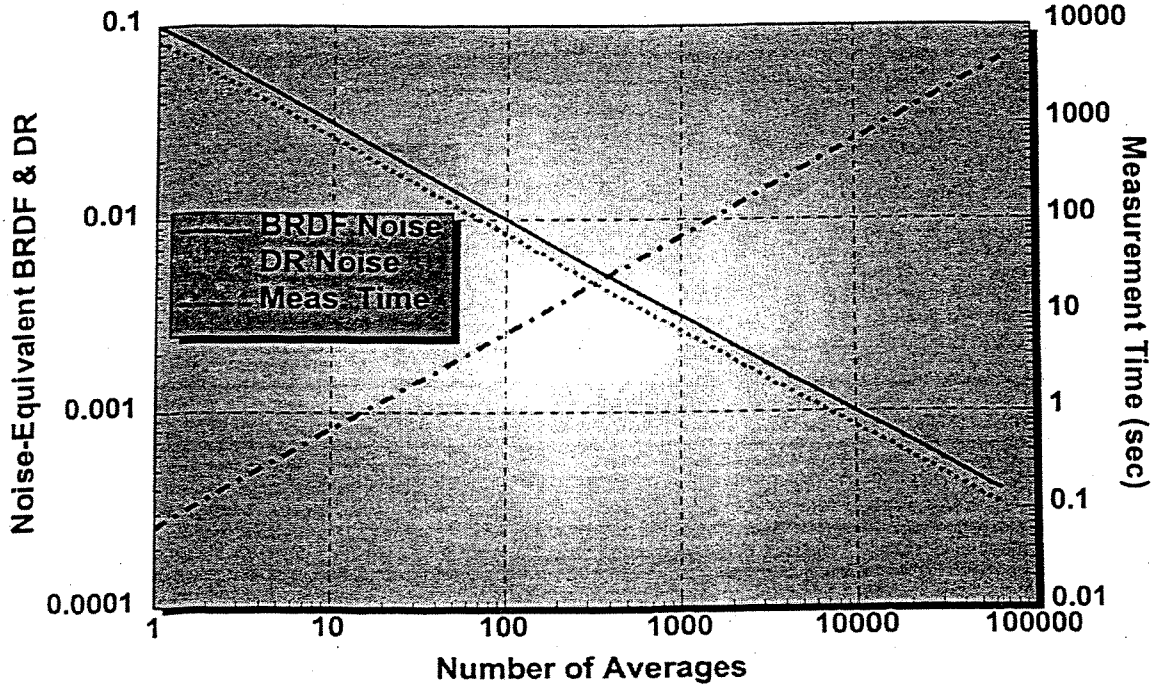

Figure 4-1. HHDR performance versus averaging. Noise equivalent BRDF and HDR fall as the square root of the number of averages, while measurement time increases linearly.

Figure 4-2 shows both the angular image and principle slice of measurement done on a diffuse gray paint at 20° incidence in the 3-5 μm band. Note the broad specular lobe. The HHDR computed directional reflectance for this sample was 12.5%, while measurement in SOC's laboratory HDR yielded a value of 14% (averaged over 3-5 μm). The main reason for the 1.5% discrepancy is that this sample showed an increase in reflectance from 5% at 3 μm to 19% at 5 μm. Averaging of the laboratory measurement was done with a constant weighting function across the band. Because the

reported value is slightly low, the HHDR's weighting function must slightly favor the shorter wavelengths. This is still good agreement, given the marked change in reflectance over this band.

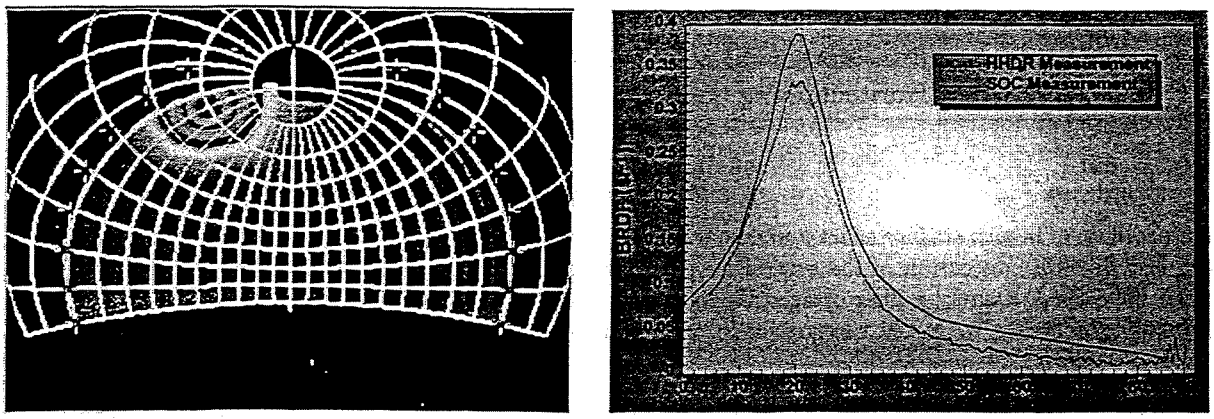

Figure 4-2. Angular image and principle BRDF slice for a gray paint sample, 20° incidence, 3-5 μm waveband. Note that SOC measured BRDF was not normalized against DR value. Typical unnormalized error is about 10%

Figure 4-3 shows the angular image and principle slice BRDF for a black paint at 75° incidence in the 8-12 μm waveband. Note the tight specular lobe visible in both the angular image and BRDF. For this sample, which displayed a nearly flat spectral reflectance across the 8-12 μm band, the HHDR reported value of 23.4% agrees well with the SOC lab measured value of 23.9%.

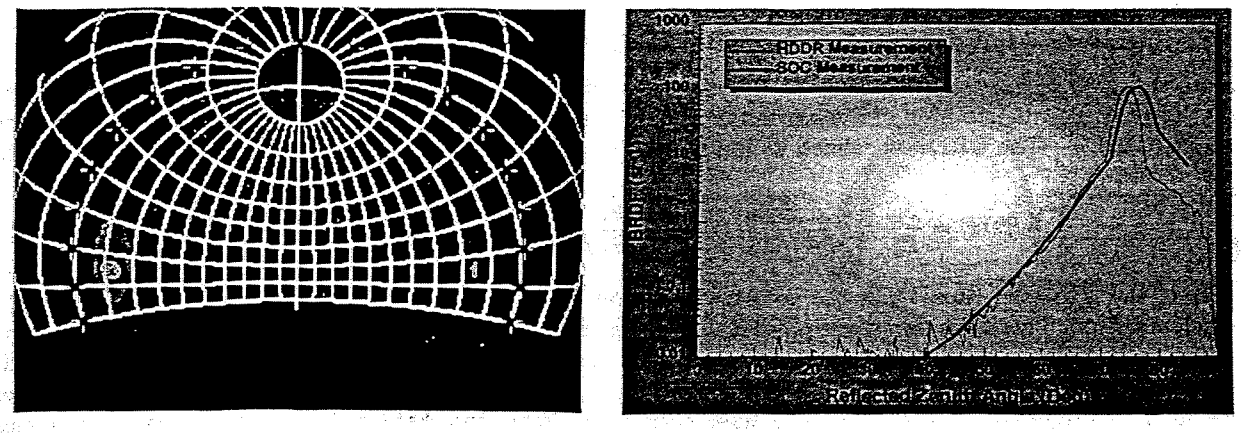

Figure 4-2. Angular image and principle BRDF slice for a black paint sample, 75° incidence, 8-12 μm waveband. Note the tight specular lobe in both the image and principle slice graph.

The HHDR, then, provides a new an powerful instrument for quantification of both BRDF and HDR *in-situ*. With this instrument, the scattering properties of materials can be visualized in a way heretofore impossible, even generating motion pictures of the change in scattering as incident azimuth or elevation is changed.

The Study on generating of BRDF table set for Multi Channel Sensor

Asako Konda, Msatoshi Yokota, Taku Nishijima , Koji Kajiwara, Yoshiaki Honda
Center for Environmental Remote Sensisng (CERES), Chiba University
1-33. Yayoi-Cho , Inage-Ku Chiba 263-8522, Japan
Tel : (81)-43-290-3845 ; Fax : (81)-43-290-3857
E-mail: Konda@rsirc.cr.chiba-u.ac.jp

Abstract
We were measuring BRDF (Bi- Directional Reflectance Distribution Factor) for the purpose of multi channel sensor analysis. For that analysis we were measuring used tower (Height is 5m) and 2 stepping motor. In this time, tower was loading a truck, and we became to get a lot of data. In due to measure these study, we could possibly that understood characteristic of grassland BRDF. First step for making BRDF table set for grassland, we discussed Composite Algorithm that avoid effects of BRDF.

1. Introduction

Recently, satellite remote sensing is becoming important engineering for measurement of environmental. However , satellite data are not only information of object, but also including another information of atmosphere, geographic and etceteras. When we used satellite data and analyze, we should remove these informations.

BRDF (Bi- Directional Reflectance Distribution Factor) is in dependent on sun Zenith angle, sun ,sensor azimuth angle, geographic information, and that dependence are different to each sensor dependence of electronic wave. If we get the truth information, we should remove some other information. And BRDF is one of some another information. Usually, we use some MODEL due to express geometry dependence of multi reflectance. But these MODELS are no suitable for using correction and estimation algorithm because these are using some parameter including difficult measurement and calculation, such as distribution of leaves.

2. Objectives

Therefore, in this study, we the measured the ground truth for Mongolia grassland, and analyzed BRDF characteristic. And we development a BRDF table set for correcting satellite data.

3. Observation

3.1 Measurement System

We used measurement system that watanable et al.,[1] developed at 1997. (Fig.1) Detail functions are shown the Table.1. And in this study, getting vegetation coverage system is change Digital video camera from 8mm video camera.

3.2 Observation

We carried out an observation the adobe system for the 23rd July to 15th August 1998 in Mongolia. Measurement areas are the three points with different vegetation coverage (Fig.2). Watanabe et al. were that one cycle of measurements every 30 degrees from 0 to 330 degrees for sensor azimuth angle and every 10 degrees from 0 degree to 60 degrees for sensor zenith angle. Total are 75 point measurements. But, by that measurement of large sensor zenith angle is less point than measurement of small sensor zenith angle. Therefore our measurement were following Table.2. Time of one cycle require about 15 minutes. It is more short time than them time because our control PC is more powerful spec than their PC.

Wavelength	350-1050nm
Spectral Resolution	0.342nm/ch(2048ch)

Integration Time	0.008-2.04 sec
Gain	1-8
Accumulation Count	1-255
FOV Angle	20 deg.
Quantization Level	16 bit
Sensor Height	1.5-5m
Sensor Azimuth Angle	0-360 deg
Sensor Zenith Angle	0-70 deg

Table.1 Measurement System.

Sensor azimuth angle [deg]	Sensor scan angle [deg]
0,30,60,90,120,150,180,210,240,270,300,330	10,20,30,40,45,50,55,60
10,20,40,50,70,80,100,110,130,140,160,170,190 200,220,230,250,260,280,290,310,320,340,350	50,55,60
0	0

Table.2 One Cycle of Measurements

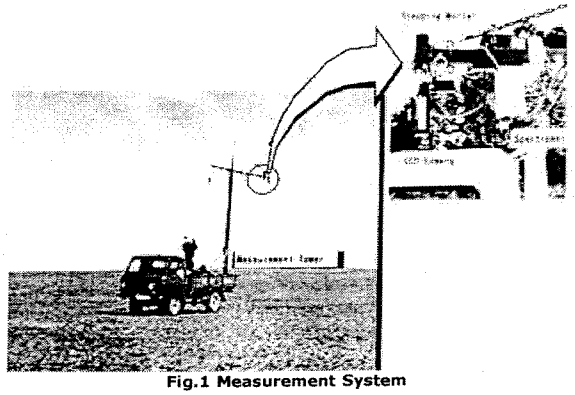

Fig.1 Measurement System

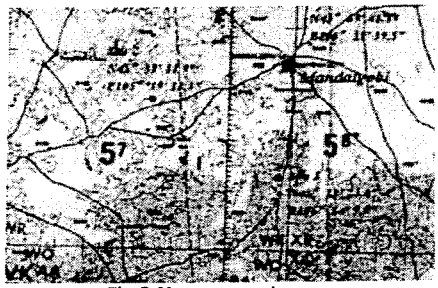

Fig.2 Measurement area

Time	Date	Count of point	Latitude	Longitude	Vegetation coverage
9:28~19:17	98/08/09	16	46'01.466	106'19.935	0.15
11:49~17:23	98/08/10	11	45'36.945	105'38.454	0.054
11:16~17:23	98/08/11	11	45'23.300	106'14.196	0.079

Table. 3 Measurement Condition